

Low-light Image Enhancement via CLIP-Fourier Guided Wavelet Diffusion

Minglong Xue
Chongqing University of Technology
China
xuemi@cqut.edu.cn

Jinhong He
Chongqing University of Technology
China
Hejh@stu.cqut.edu.cn

Yanyi He
Chongqing University of Technology
China
yui@stu.cqut.edu.cn

Zhipu Liu
Chongqing University of Technology
China
zpliu@cqut.edu.cn

Wenhai Wang
The Chinese University of Hong Kong
Hong Kong
whwang@ie.cuhk.edu.hk

Mingliang Zhou
Chongqing University
China
mingliangzhou@cqu.edu.cn



Figure 1. Visual comparison of our method with the SOTA unsupervised method SCI and two supervised methods, SNRNet and WCDM, in low-light image enhancement. While the previous methods suffer from color distortion and generate chaotic content, our method effectively improves the enhancement and can generate images similar to the original ones.

Abstract

Low-light image enhancement techniques have significantly progressed, but unstable image quality recovery and unsatisfactory visual perception are still significant challenges. To solve these problems, we propose a novel and robust low-light image enhancement method via CLIP-Fourier Guided Wavelet Diffusion, abbreviated as CFWD. Specifically, we design a guided network with a multiscale visual language in the frequency domain based on the wavelet transform to achieve effective image enhancement iteratively. In addition, we combine the advantages of Fourier transform in detail perception to construct a hybrid frequency domain space with significant perceptual capabilities (HFDPM). This operation guides wavelet diffusion to recover the fine-grained structure of the image and avoid diversity confusion. Extensive quantitative and qualitative experiments on publicly available real-world benchmarks show that our method outperforms existing state-of-the-art methods and better reproduces images similar to normal images. Code is available at <https://github.com/He-Jinhong/CFWD>.

Keywords: Low-Light Image Enhancement, Diffusion Models, CLIP, Fourier Transform, Wavelet Transform.

1 INTRODUCTION

Images captured in low-light environments are one of the key factors affecting downstream tasks [Li et al. 2021b; Xue et al. 2020], and it remains a challenge to enhance low-light images effectively. Early low-light image enhancement methods focused on optimizing the parameters of the image, and their effectiveness relied heavily on the accuracy of the hand-crafted priori. However, low-light image enhancement is an ill-posed problem, making it challenging to adapt a priori to various lighting conditions in open scenes. The field of image low-light enhancement has seen new opportunities with the emergence of deep learning. Currently, the learning-based approach to establish a direct mapping relationship between low-light images and normal images for enhancement learning has better performance, especially the distortion metrics such as PSNR and SSIM [Wei et al. 2018], which have significantly improved.

In addition, the recent emergence of diffusion models [Song and Ermon 2019; Song et al. 2020b] has attracted much attention in image restoration due to their generative solid and generalization capabilities. However, Diffusion models still have considerable challenges for low-light image enhancement. The patch-based diffusion model WeatherDiff [Özdenizci and Legenstein 2023] can trigger redundant

chaotic information due to the diversity of randomly sampled Gaussian noise in the inference process. The wavelet-domain-based diffusion models WCDM [Jiang et al. 2023] can also cause the loss of pixel information due to the randomness of the inference process as well as the loss of details triggered by wavelet transforms so that it is difficult to recover the original image effect, as shown in Fig. 1. As far as I know, these diffusion models ignore the constraint-guiding ability of visual-language prompts in low-light image enhancement. Moreover, with the steady development of large models, nature language has been proven to have great potential in the visual domain.

Therefore, We propose a wavelet diffusion model supervised by the semantic capabilities of large scale Contrastive-Language-Image-Pretraining (CLIP) models and Fourier transform guided for robust and efficient low-light image enhancement. Specifically, The underlying network framework is constructed through WCDM [Jiang et al. 2023]. Based on the frequency-domain spatial of the wavelet transform and the semantic capability of the CLIP, we design a bootstrap network with multiscale visual-language to realize effective image enhancement step by step. In addition, we combine the advantages of the Fourier transform for detail perception to construct a hybrid frequency domain space with significant perceptual capability, which complements the image restoration effect at the fine-grained level and avoids the confusion of content and diversity, thus further guiding the diffusion restoration in the wavelet domain. As shown in Fig. 1, Our method improves light distribution and global contrast, resulting in better visual recovery compared to current popular methods. Concurrently, Extensive experiments on publicly available datasets demonstrate that our method surpasses existing state-of-the-art (SOTA) methods in distortion and perceptual metrics. Our contributions can be summarized as follows:

- We successfully introduce multimodal visual-language information in a diffusion model-based low-light image enhancement method. We also propose the CLIP-Fourier guided Wavelet Diffusion model (CFWD) to recover low-light images with more realistic visual perception.
- We propose a novel hybrid frequency domain perception module based on wavelet and Fourier to construct a hybrid frequency domain space with significant information perception capability. The module can effectively recover high-frequency information and enhance image details.
- We further design a multiscale visual-language guidance network for progressive natural language guidance through the multilevel frequency domain space generated by wavelet transform. This approach achieves multilevel constraints on the enhancement process,

further preventing the generalization of chaotic information and effectively improving the enhancement effect.

- As demonstrated by experimental results on public benchmark datasets, our proposed method significantly improves image quality assessment up to SOTA while also possessing better visual results.

2 RELATED WORK

2.1 Low-light Image Enhancement

Traditional approaches focus on processing using information from the image itself, such as the use of filters, histogram equalization, Retinex theory, and other means of achieving image enhancement [Fu et al. 2016; Li et al. 2018; Lin and Shi 2014; Park et al. 2022]. With the proven benefits of deep learning in numerous low-level visual tasks, low-light image enhancement has been added to the study of learning-based methods [Mao et al. 2016; Sun et al. 2015]. EnlightenGAN [Jiang et al. 2021] was first trained with unpaired images using a generative inverse network as the main framework. Zero-DCE [Guo et al. 2020] constructed a pixel-level curve-estimating convolutional neural network by stepwise derivation, and A series of zero-reference training loss functions were designed. RUAS [Liu et al. 2021] designed a Retinex architecture-based search unfolding technique. SNRNet [Xu et al. 2022] utilized a signal-to-noise ratio-aware transformer and a CNN model with spatially varying operations for recovery.

2.2 Diffusion Model for Image Restoration

Diffusion models have achieved excellent results in image generation by employing parametric Markov chains to optimize the likelihood function's lower variational bounds, allowing them to generate more accurate target distributions than other generative models (i.e., GANs). Therefore, many image restoration tasks are also introduced into the diffusion model, such as super-resolution [Luo et al. 2023], restoration [Lugmayr et al. 2022], and deblurring [Ren et al. 2022]. For the low-light image enhancement task, WCDM [Jiang et al. 2023] combined the wavelet transform and the diffusion model to design an efficient and robust diffusion recovery framework.

2.3 CLIP in Vision

Recently, CLIP has shown remarkable results in zero-shot classification and various visual tasks [Kuo et al. 2022; Zang et al. 2022; Zhou et al. 2022], thanks to the knowledge gained from large-scale image-text data. Meanwhile, Recent studies [Liang et al. 2023; Wang et al. 2023] have shown that the visual language embedded in CLIP can assess image quality and abstraction perception. These studies inspire our work, and we propose a method to combine the semantic features of the CLIP pre-trained model with wavelet diffusion to create a hybrid frequency domain space. This approach significantly

reduces the uncontrollability of the input diffusion process and information loss, establishing the SOTA criterion for low-light image enhancement and surpassing the potency of existing methods.

3 METHODOLOGY

The overall framework of our proposed CFWD is shown in Fig. 1. Inspired by WCDM [Jiang et al. 2023], our work decomposes the input image into global and high-frequency information by wavelet transform and performs diffusion operation on the global wavelet domain. At the same time, we compute the text-image similarity between the prompt information and the enhanced global information through a frozen CLIP model. Also, we use a hybrid based on wavelet and Fourier perceptual frequency domain module to improve the structural similarity between the recovered and normal images. Finally, the enhancement results are recovered through our predefined nature language prompts to guide the recovery until visually satisfactory results are obtained. We describe the main components of our approach in further detail below.

3.1 Wavelet Diffusion Model

Diffusion models [Ho et al. 2020; Song et al. 2020a] aim to learn Markov chains, which are usually divided into two stages: forward diffusion and denoising inference. Using fixed variance $\{\beta_t \in (0, 1)\}_{t=1}^T$, its forward diffusion process can continuously add Gaussian noise to the input distribution. And the inverse process recovers the original data from Gaussian noise; our goal is to use the synthetic data to optimize the noise predictor to learn the conditional denoising process $p_\theta(\hat{x}_{0:T}|\tilde{x})$ and transform the randomly sampled Gaussian noise $\hat{x}_T \sim N(0, I)$ into the exact result \hat{x}_0 .

Besides, the Wavelet Diffusion Model performs diffusion inference on the global information from the wavelet transform of the image, and it does so by giving a low-light input image $I_{Low} \in R^{H \times W \times C}$. We transform the input low-light image K times using the multidimensional discrete wavelet transform (K-DWT), and decompose it into four subbands each time, i.e.,

$$\{A_L^K, V_L^K, H_L^K, D_L^K\} = K - DWT(I_{Low}) \quad (1)$$

Where $A_L^K, V_L^K, H_L^K, D_L^K$ denote the global information and the high-frequency information in the vertical, horizontal, and diagonal directions of the input image after k wavelet transforms, respectively.

Furthermore, the WCDM [Jiang et al. 2023] performs both forward diffusion and denoising processes in the training phase and achieves content consistency by optimizing the noise predictor to obtain the recovered global information \hat{A}_L^K and finally inducing the minimization of the $L2$ distance

between the recovered global information \hat{A}_L^K and the standard global information \hat{A}_H^K that is available only in the training phase, which can be described as:

$$\mathcal{L}_{L2} = \|\hat{A}_L^K - \hat{A}_H^K\|^2 \quad (2)$$

Accordingly, the loss function used to optimize the wavelet-based diffusion model can be summarised as follows:

$$\mathcal{L}_{diff} = E_{t \sim [1, T]} E_{x_0 \sim p(x_0)} E_{z_t \sim N(0, I)} \|z_t - z_\theta(x_t, \tilde{x}, t)\|^2 + \mathcal{L}_{L2} \quad (3)$$

3.2 Multiscale Visual-Language Guidance Network

By combining multiple frequency domain images generated by the wavelet transform, we divide the enhancement process into multiple prompts hierarchies to guide the enhancement of low-light images. Firstly, we take the global information A_L^K and A_L^{K-1} captured by multiple wavelet transforms and guide it through the prompts pairs $T_i = \{T_p, T_n\}$ (T_p denotes a positive prompt and T_n denotes a negative prompt) for the restoration of the excellent illumination, to induce the transformed global information to get more illumination similarity with that of the standard image, and to train the enhancement network, We use the cosine similarity loss of CLIP. i.e.,

$$\mathcal{L}_{ALE} = \frac{\cos(\Phi_{image}(A_L^K), \Phi_{text}(T_n))}{\cos(\Phi_{image}(A_L^K), \Phi_{text}(T_p)) + \cos(\Phi_{image}(A_L^{K-1}), \Phi_{text}(T_p))} \quad (4)$$

Where Φ_{text} is the text encoder, and Φ_{image} is the image encoder. First, well-recovered global information is obtained by natural language prompt guidance in the pre-frequency domain space. Then, fusing the recovered high-frequency features yields an initial enhanced image. Finally, the global structure of the initial enhanced image is guided by the pre-trained positive/negative prompts. To train the network, we use the similarity \mathcal{L}_{CLIP} between the metric enhancement result and the prompts in CLIP space, i.e.:

$$\mathcal{L}_{CLIP} = \frac{e^{\cos(\Phi_{image}(I_E), \Phi_{text}(T_n))}}{\sum_{i \in \{T_n, T_p\}} e^{\cos(\Phi_{image}(I_E), \Phi_{text}(T_i))}} \quad (5)$$

Meanwhile, to ensure the accuracy of nature language guidance, we perform MSE loss [Liang et al. 2023] between the enhanced image I_E and the standard image I_H to ensure that its structure can maintain better similarity with the original image during nature language guided. i.e.,

$$\mathcal{L}_{MSE} = \sum_{l=0}^4 \gamma_l \|\Phi_{image}^l(I_E) - \Phi_{image}^l(I_H)\|^2 \quad (6)$$

Thus, we can summarize the CLIP loss as:

$$\mathcal{L}_{mse} = \mathcal{L}_{ALE} + \mathcal{L}_{CLIP} + \mathcal{L}_{MSE} \quad (7)$$

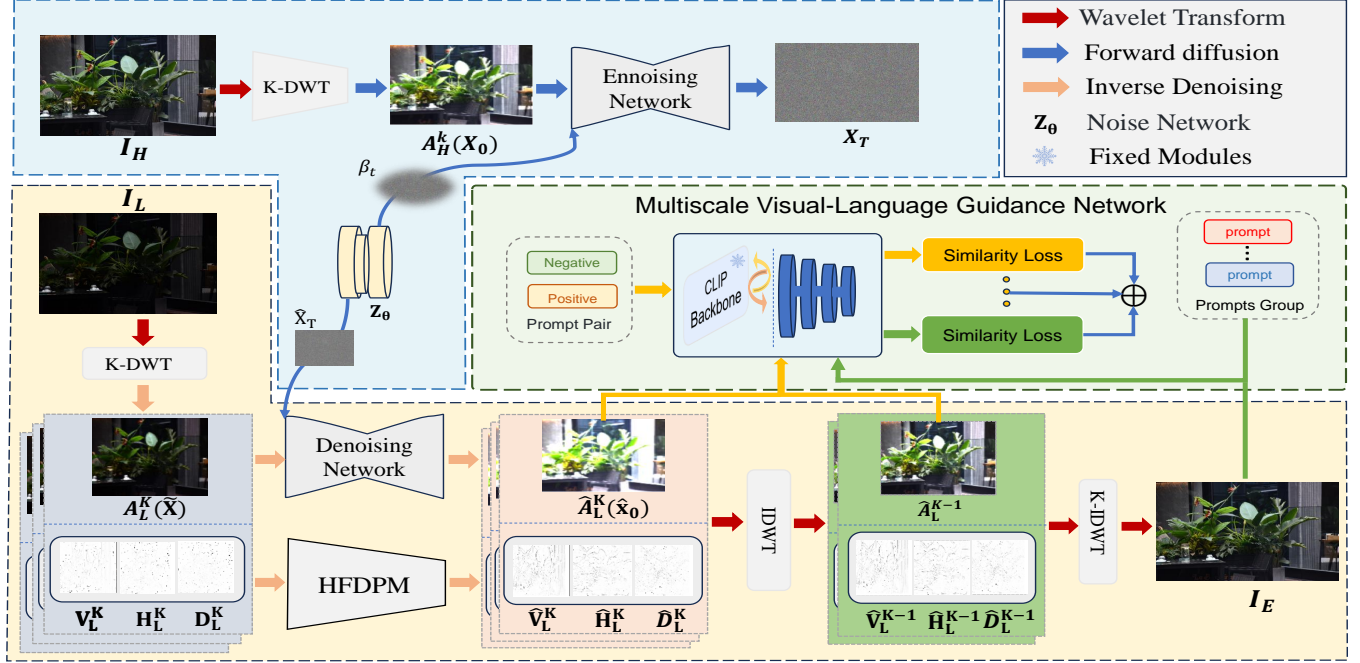


Figure 2. The proposed overall framework for CFWD. We first perform the K-wavelet transform on the I_L and I_H to obtain the global information A_L^K and high-frequency information $\{V_L^K, H_L^K, D_L^K\}$. The global information of the image can be initially recovered by diffusion inference operation on A_L^K . The Hybrid Frequency Domain Perception Module (HFDPM) recovers the high-frequency information of each transform more efficiently. Then, the inverse discrete wavelet transform transforms the processed high-frequency and global information. After the transformation, \hat{A}_L^{K-1} and \hat{A}_L^K are then fed into a multi-scale visual-language network for semantically guided recovery with the initial prompt pairs, and the image I_E can be initially recovered after semantically co-guided through the multi-scale, and finally I_E is guided with the trained prompt group to obtain the recovered image close to the original image.

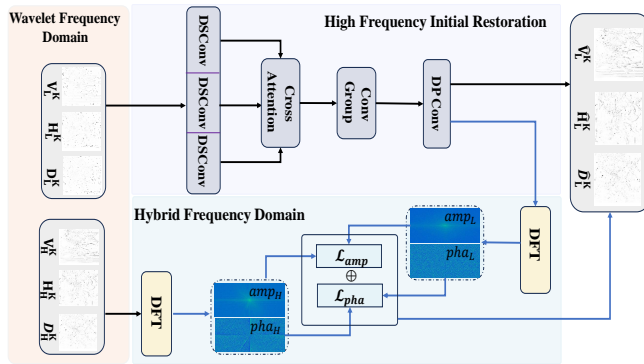


Figure 3. The detailed architecture of our proposed Hybrid Frequency Domain Perception Module. DFT denotes Discrete Fourier Transform on top of Wavelet Transform.

Where γ_l is the weight of layer l of the image encoder in the ResNet101 CLIP model. w_1 and w_2 balance the weights for different loss term sizes and are empirically set to 0.7 and 0.9, respectively.

3.3 Hybrid Frequency Domain Perception Module

In this paper, we design a specific framework of the hybrid frequency domain perception module as shown in Fig 3. The high-frequency coefficients generated by the wavelet transform of the low-light image retain the original image's detailed features to the greatest extent possible. After recovering the high-frequency restoration module [Hai et al. 2022; Jiang et al. 2023], can obtain initial high-frequency recovery coefficients. For this purpose, we use the high-frequency information recovery loss \mathcal{L}_{WHF} , which is similar to WCDM [Jiang et al. 2023]. We can show with the following function:

$$\mathcal{L}_{WHF} = \eta_1 \sum_{k=1}^K \|\{\hat{V}_L^K, \hat{H}_L^K, \hat{D}_L^K\} - \{V_L^K, H_L^K, D_L^K\}\|^2 + \eta_2 \sum_{k=1}^K TV(\{\hat{V}_L^K, \hat{H}_L^K, \hat{D}_L^K\}) \quad (8)$$

In addition, the high-frequency coefficients recovered from the low-light image are obtained by Fourier transform $fre(\cdot)$ to get their corresponding magnitude and phase (amp_L, pha_L). The same method is used to get the magnitude and phase of

the high-frequency coefficients of the normal image (amp_H, pha_H), network. Specifically, the LOLv2-Real_captured dataset contains 689 low/normal light image pairs for training and 100 for testing. Most low-light images were collected by varying the exposure time and ISO and fixing other camera parameters. The LSRW dataset contains 5,650 image pairs captured in a variety of scenarios. 5,600 image pairs were randomly selected as the training set, and the remaining 50 pairs were used for evaluation. To evaluate the generalization ability of the proposed method in this paper, we tested our method on the BAID [Lv et al. 2022] test dataset, which consists of 368 backlit images with 2K resolution. In addition, we also tested on two unpaired datasets, LIME [Guo et al. 2016] and DICM [Lee et al. 2013].

$$amp_L, pha_L = fre(\{\hat{V}_L^K, \hat{H}_L^K, \hat{D}_L^K\}) \quad (9)$$

$$amp_H, pha_H = fre(\{V_H^K, H_H^K, D_H^K\}) \quad (10)$$

To further obtain a recovery image that matches human perception, the proposed method employs L_1 loss to minimize the information difference between the spectrograms of high-frequency coefficients of the normal image and the spectrograms of the low-light image, which is expressed as:

$$\mathcal{L}_{fre} = \vartheta_1 \mathcal{L}_{amp} + \vartheta_2 \mathcal{L}_{pha} \quad (11)$$

$$\mathcal{L}_{amp} = \frac{1}{K} \sum_{i=1}^K \| amp_L^i - amp_H^i \| \quad (12)$$

$$\mathcal{L}_{pha} = \frac{1}{K} \sum_{i=1}^K \| pha_L^i - pha_H^i \| \quad (13)$$

Where ϑ_1 and ϑ_2 are the weighting parameters for the amplitude and phase losses, and i is the scale of the current wavelet transform, so the total loss in the Hybrid Frequency domain space can summarize as:

$$\mathcal{L}_{HFDPM} = \vartheta_1 \mathcal{L}_{WHF} + \vartheta_2 \mathcal{L}_{fre} \quad (14)$$

3.4 Model Training

Moreover, to optimize the diffusion model, visual-language guided network, and the objective function in the frequency domain space. We finally also optimize \mathcal{L}_{HFDPM} by combining L_1 loss and SSIM loss [Wang et al. 2004] again for content loss. To minimize the content difference between the recovered image I_E and the reference image I_H , i.e

$$\mathcal{L}_{element} = |\Phi_{image}(I_E) - \Phi_{image}(I_H)| + (1 - SSIM(I_E, I_H)) \quad (15)$$

Combining multiple losses and CLIP loss weights can restore the content structure of normal images to a large extent and stabilize the recovery prompted by natural language. Its total loss can be expressed as:

$$\mathcal{L}_{All} = \mathcal{L}_{diff} + \mathcal{L}_{CLIP} + \mathcal{L}_{HFDPM} + \mathcal{L}_{element} \quad (16)$$

4 EXPERIMENTS

4.1 Experimental Settings

Dataset. Our network is trained and evaluated on the LOLv1 dataset [Wei et al. 2018], which contains 500 real-world low/normal light image pairs, of which 485 image pairs are used for training and 15 image pairs are used for evaluation. In addition, we employ two other real-world pairwise datasets, LOLv2-Real_captured [Yang et al. 2021], and LSRW [Hai et al. 2023], to evaluate the performance of our proposed

Training. In this article. We implement our method with PyTorch on two NVIDIA RTX 3090 GPUs. The network was set up with a total of 2×10^5 iterations, using the Adam optimizer, with the initial learning rate set to 1×10^{-4} , and the batch size and patch size are set to 16 and 256×256 , respectively, we set the number of wavelet transforms to 2 and the CLIP loss weight to 1×10^3 .

Evaluation Metrics. For the real-world paired datasets we tested, we propose to use two full-reference distortion metrics, PNSR and SSIM [Wang et al. 2004], and two perceptual metrics LPIPS [Zhang et al. 2018] and FID [Heusel et al. 2017], to evaluate the performance and visualization of our method, for the unpaired datasets LIME and DICM. We use two non-reference perceptual metrics, NIQE [Mittal et al. 2012b] and BRISQUE [Mittal et al. 2012a] for evaluation.

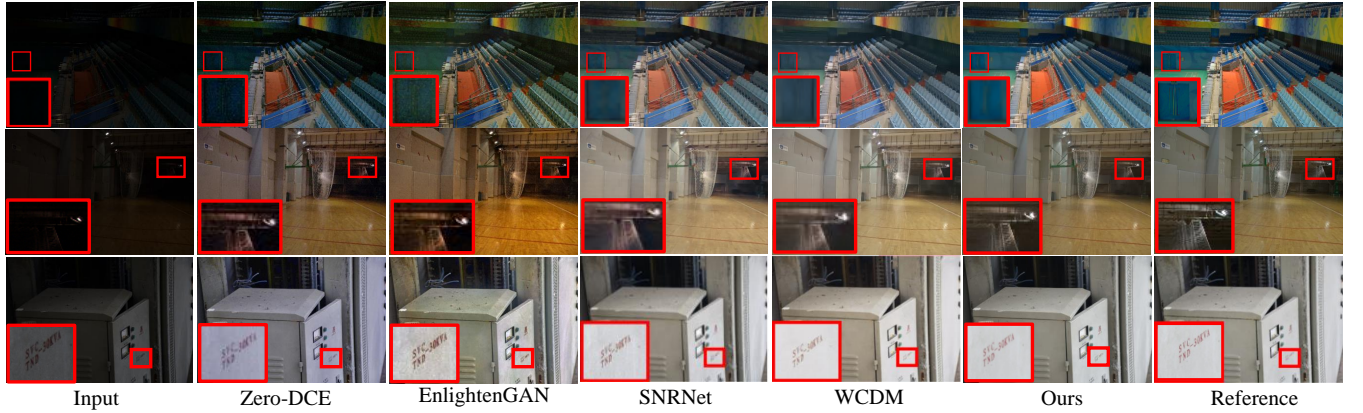
Comparison Methods. To verify the effectiveness of the method proposed in this paper, we compared it with the SOTA methods in recent years, including RetinexNet [Wei et al. 2018], DSLR [Lim and Kim 2020], DRBN [Yang et al. 2020], Zero-DCE [Guo et al. 2020], Zero-DCE [Li et al. 2021a], MIRNet [Zamir et al. 2020], EnlightenGAN [Jiang et al. 2021], ReLLIE [Zhang et al. 2021], RUAS [Liu et al. 2021], DDIM [Song et al. 2020a], SCI [Ma et al. 2022], URetinex-Net [Wu et al. 2022], SNRNet [Xu et al. 2022], Palette [Saharia et al. 2022], Uformer [Wang et al. 2022], Restormer [Zamir et al. 2022], CDEF [Lei et al. 2022], UHDFour [Li et al. 2023], WeatherDiff [Özdenizci and Legenstein 2023], GDP [Fei et al. 2023], CLIP-LIT [Liang et al. 2023], and WCDM [Jiang et al. 2023].

4.2 Results

Quantitative Comparison. Firstly, we compare our method with all comparative methods on the LOLv 1 [Wei et al. 2018], LOLv2-Real_captured [Yang et al. 2021], and LSRW [Hai et al. 2023] test sets. As shown in Table 1, our method achieves SOTA quantitative performance in several metrics compared to all compared methods. Among them, for the distortion metrics, we are ahead of the current SOTA methods across the board, implying that our results have more high-frequency detail and structure. Specifically, for the distortion metrics, compared to the second-best method,

Table 1. Quantitative evaluation of different methods on LOLv1 [Wei et al. 2018], LOLv2-Real_captured [Yang et al. 2021], and LSRW datasets [Hai et al. 2023]. The best and second performance are marked in red and blue, respectively.

Methods	Reference	LOLv1				LOLv2-Real_captured				LSRW			
		PSNR↑	SSIM↑	LPIPS↓	FID↓	PSNR↑	SSIM↑	LPIPS↓	FID↓	PSNR↑	SSIM↑	LPIPS↓	FID↓
RetinexNet	BMVC'18	16.774	0.462	0.417	126.266	17.715	0.652	0.436	133.905	15.609	0.414	0.454	108.350
DSLR	TMM'20	14.816	0.572	0.375	104.428	17.000	0.596	0.408	114.306	15.259	0.441	0.464	84.930
DRBN	CVPR'20	16.774	0.462	0.417	126.266	18.466	0.768	0.352	89.085	16.734	0.507	0.457	80.727
Zero-DCE	CVPR'20	14.816	0.572	0.375	104.428	18.059	0.580	0.352	80.449	15.867	0.443	0.411	63.320
MIRNet	ECCV'20	24.138	0.830	0.250	69.179	20.020	0.820	0.233	49.108	16.470	0.477	0.430	93.811
EnlightenGAN	TIP'21	17.606	0.653	0.372	94.704	18.676	0.678	0.364	84.044	17.106	0.463	0.406	69.033
ReLLIE	ACM MM'21	11.437	0.482	0.375	95.510	14.400	0.536	0.334	79.838	13.685	0.422	0.404	65.221
RUAS	CVPR'21	16.405	0.503	0.364	101.971	15.351	0.495	0.395	94.162	14.271	0.461	0.501	78.392
DDIM	ICLR'21	16.521	0.776	0.376	84.071	15.280	0.788	0.387	76.387	14.858	0.486	0.495	71.812
CDEF	TMM'22	16.335	0.585	0.407	90.620	19.757	0.630	0.349	74.055	16.758	0.465	0.399	62.780
SCI	CVPR'22	14.784	0.525	0.366	78.598	17.304	0.540	0.345	67.624	15.242	0.419	0.404	56.261
URetinex-Net	CVPR'22	19.842	0.824	0.237	52.383	21.093	0.858	0.208	49.836	18.271	0.518	0.419	66.871
SNRNet	CVPR'22	24.610	0.842	0.233	55.121	21.480	0.849	0.237	54.532	16.499	0.505	0.419	65.807
Uformer	CVPR'22	19.001	0.741	0.354	109.351	18.442	0.759	0.347	98.138	16.591	0.494	0.435	82.299
Restormer	CVPR'22	20.614	0.797	0.288	72.998	24.910	0.851	0.264	58.649	16.303	0.453	0.427	69.219
Palette	SIGGRAPH'22	11.771	0.561	0.498	108.291	14.703	0.692	0.333	83.942	13.570	0.476	0.479	73.841
UHDFour	ICLR'23	23.093	0.821	0.259	56.912	21.785	0.854	0.292	60.837	17.300	0.529	0.443	62.032
WeatherDiff	TPAMI'23	17.913	0.811	0.272	73.903	20.009	0.829	0.253	59.670	16.507	0.487	0.431	96.050
GDP	CVPR'23	15.896	0.542	0.421	117.456	14.290	0.493	0.435	102.416	12.887	0.362	0.412	76.908
WCDM	TOG'23	26.336	0.845	0.217	48.114	28.857	0.876	0.207	45.359	19.281	0.552	0.350	45.294
CFWD(Ours)	-	29.212	0.872	0.197	40.987	29.855	0.890	0.193	34.814	19.566	0.572	0.374	47.606

**Figure 4.** Visual comparison of our method with SOTA methods on LOLv1 [Wei et al. 2018](row 1), LOLv2-Real_captured [Yang et al. 2021](row 2), and LSRW [Hai et al. 2023](row 3) datasets from various years in recent years. Our method is closer to a normal image, best viewed by zooming in.

WCDM, our method achieves a performance of $2.876dB(= 29.212 - 26.336)$ for PSNR and $0.027(= 0.872 - 0.845)$ improvements with SSIM. We have similarly significant improvements on the LOLv2-Real_captured test set, i.e., $0.998dB(= 29.855 - 28.857)$ and $0.014(= 0.890 - 0.876)$. On the LSRW test set, our method improves these two metrics by at least $0.285dB(= 19.566 - 19.281)$ and $0.020(= 0.572 - 0.552)$, respectively. For the perceptual metrics, i.e., LPIPS and FID, we improved considerably compared to the second-best method, WCDM, on the LOLv1 test set and the LOLv2-Real_captured test set. Specifically, there were reductions of $0.02(= 0.217 - 0.197)$ and $0.014(= 0.207 - 0.193)$ in LPIPS, and substantial improvements of $7.127(= 48.114 - 40.987)$ and $10.545(=$

$45.359 - 34.814)$ in FID, respectively. We also achieved the second-best evaluation on the LSRW test set, which suggests that the method proposed in this paper can produce recovered images with satisfactory visual quality, further demonstrating the effectiveness of our approach. Furthermore, a quantitative comparison of the BAID [Lv et al. 2022] test dataset is shown in Table 3. Our method outperforms all SOTA methods in the evaluation metrics demonstrating the generalization ability of the proposed method and high-resolution low-light image recovery is more effective.

Meanwhile, we performed evaluation comparisons with competing methods on two unpaired datasets to validate the

Table 2. Quantitative comparison of 2K resolution backlight images from the BAID [Lv et al. 2022] dataset.

Methods	Reference	PSNR↑	SSIM↑	LPIPS↓	FID↓
Zero-DCE++	TPAMI'21	16.021	0.832	0.240	47.030
EnlightenGAN	TIP'21	17.957	0.866	0.125	47.045
SCI	CVPR'22	16.639	0.768	0.197	41.458
SNRNet	CVPR'22	17.010	0.754	0.398	63.463
UHDFour	ICLR'23	18.541	0.713	0.319	36.025
CLIP-LIT	ICCV'23	21.611	0.883	0.159	27.926
WCDM	TOG'23	26.042	0.915	0.130	15.870
CFWD(Ours)	-	26.918	0.917	0.118	14.852

Table 3. Quantitative comparison on LIME [Guo et al. 2016] and DICM [Lee et al. 2013] datasets. Our method performs the best consistently.

Methods	Reference	DICM		LIME	
		NIQE↓	BRISQUE↓	NIQE↓	BRISQUE↓
DRBN	CVPR'20	4.369	30.708	4.562	34.564
Zero-DCE	CVPR'20	3.951	23.350	4.379	26.054
MIRNet	ECCV'20	4.021	22.104	4.378	28.623
EnlightenGAN	TIP'21	3.832	19.129	4.249	22.664
RUAS	CVPR'21	7.306	46.882	5.322	34.880
DDIM	ICLR'21	3.899	19.787	3.899	24.474
SCI	CVPR'22	4.519	27.922	4.399	25.170
URetinet-Net	CVPR'22	4.774	24.544	4.694	29.022
SNRNet	CVPR'22	3.804	19.459	4.597	29.023
UHDFour	ICLR'23	4.575	26.926	4.430	20.263
GDP	CVPR'23	4.358	19.294	4.891	27.460
WCDM	TOG'23	3.806	18.584	3.777	19.843
CFWD(Ours)	-	3.566	17.403	3.628	15.138

effectiveness and generalization of our method. We evaluated the effectiveness of our method against visual quality by combining two non-reference perception metrics, NIQE [Mittal et al. 2012 b] and BRISQUE [Mittal et al. 2012 a], where lower metrics imply better visual quality. As shown in Table 4, our method obtains the best results in both datasets compared to other competing methods, proving that our method has better generalization ability in real scenarios.

Visual Comparison. Fig. 4 is shown the compare our method with SOTA methods on the paired dataset. Since there are space constraints, we only show the results of the better-performing method for each year. The images in rows 1-3 are selected from the LOLv1, LOLv2-Real_captured, and LSRW test sets. The visualization of the BAID dataset is then shown in Fig. 5. These comparisons make it easy to see that previous methods appear to have incorrect exposure, color distortion, noise amplification, or artifacts, undermining overall visual quality. e.g., EnlightenGAN and SCI suffer from generating artifacts and noise amplification, while SNRNet and WCDM color distortion. In contrast, our method consistently produces visually pleasing results with improved color and brightness without overexposure or underexposure. In addition, our method has less damage to the recovered content structure. It effectively improves global

Table 4. Results of an ablation study at the prompt network scale.

Prompt Scale	PSNR↑	SSIM↑	LPIPS↓	FID↓
M=1	27.809	0.866	0.225	48.501
M=2	28.512	0.871	0.216	43.167
M=3	29.212	0.872	0.197	40.987

and local contrast, reconstructing sharper details and resulting in a visual result that more closely resembles the original image. More results are shown in the appendix at the end.

We also visually compare our method and the competing methods on the unpaired dataset in Fig. 6, where the data in image rows 1-2 are selected from the DICM and LIME datasets, respectively. Compared to our method, Zero-DCE, EnlightenGAN exhibits more cluttered content, and SNRNet results in severe distortions, whereas WCDM overexposes the recovered images. Moreover, our results exhibit better color contrast and input-output consistency in well-lit areas.

4.3 Ablation Study

In this subsection, we conduct ablation studies on multiscale visual-language guided networks and hybrid frequency domain perception modules to explore the most appropriate parameter pairings for the networks. We evaluate their performances on the LOLv1 [Wei et al. 2018] test set for analysis. Detailed experiment settings are discussed below.

Prompt Scale. To investigate the effect of the level M of the visual-language guided network on our method, When the wavelet transform scale is 2, we tested the effect of different M on enhancing the result I_E , as shown in Table 4, the performance of the model steadily improves with the gradual increase of M. This suggests that multiscale prompt information can better guide network optimization and prevent the instability of the model against diffusion.

Table 5. Ablation studies of the optimal effectiveness of our Hybrid Frequency Domain Perception Module.

Versions	PSNR↑	SSIM↑	LPIPS↓	FID↓
HFDPM_v1	27.638	0.862	0.215	43.193
HFDPM_v2	28.282	0.868	0.209	41.185
HFDPM_v3	29.212	0.872	0.197	40.987

Hybrid Frequency Domain Perception Module. Since significant differences exist in the feature information contained in the frequency domain space at different stages, we have done a series of experimental tests to form three HFDPM versions, as shown in Table 5. Specifically, HFDPM_v1 utilizes the wavelet domain of the global information to perform a Fourier transform to capture the detailed features, HFDPM_v2 uses only the high-frequency coefficients of the first wavelet transform to form a Hybrid-frequency domain to capture detailed information, and HFDPM_v3

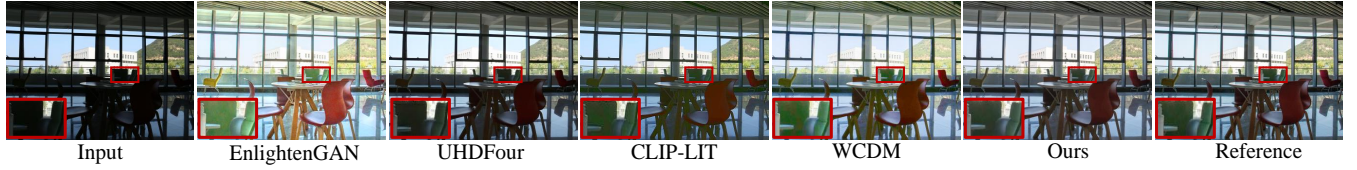


Figure 5. Visual comparison of 2K resolution backlight images of our method and competing methods on BAID [Lv et al. 2022] test set. It is best viewed by zooming in.

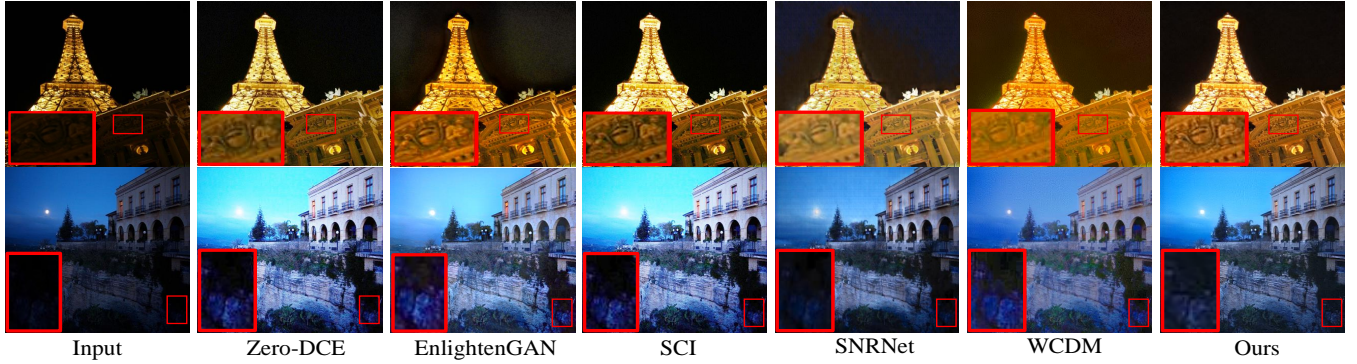


Figure 6. Visual comparison on the DICM [Lee et al. 2013] (row 1), LIME [Guo et al. 2016] (row 2) datasets among SOTA low-light image enhancement approaches.

performs Fourier transform of all the high-frequency coefficients obtained by wavelet transform to form a multi-group hybrid frequency domain space. It effectively the acquisition of high-frequency features by combining the multi-group hybrid frequency domain space. The results demonstrate that the multi-group hybrid frequency domain of HFDPM_v3 has significant perceptual ability for high-frequency features and can recover the original image effect highly.

5 CONCLUSIONS

We successfully introduced visual-language information into diffusion modeling for low-light image enhancement. We have presented a wavelet diffusion model based on CLIP and Fourier transform supervision, which utilizes the generative power of diffusion models and the a priori nature of natural language information to enhance the recovery of visual perception significantly. In addition, we design a novel hybrid frequency-domain perception module that enhances the recovery of high-frequency information by combining the advantages of wavelet transform and Fourier transform in information perception to effectively the content structure of the recovered and normal images. Experimental results on publicly available benchmarks show that our method outperforms competitors in comprehensive evaluation while providing better stability and generalizability.

References

- Ben Fei, Zhaoyang Lyu, Liang Pan, Junzhe Zhang, Weidong Yang, Tianyue Luo, Bo Zhang, and Bo Dai. 2023. Generative Diffusion Prior for Unified Image Restoration and Enhancement. In *Proceedings of the IEEE/CVF Conference on Computer Vision and Pattern Recognition*. 9935–9946.
- Xueyang Fu, Delu Zeng, Yue Huang, Xiao-Ping Zhang, and Xinghao Ding. 2016. A weighted variational model for simultaneous reflectance and illumination estimation. In *Proceedings of the IEEE conference on computer vision and pattern recognition*. 2782–2790.
- Chunle Guo, Chongyi Li, Jichang Guo, Chen Change Loy, Junhui Hou, Sam Kwong, and Runmin Cong. 2020. Zero-reference deep curve estimation for low-light image enhancement. In *Proceedings of the IEEE/CVF conference on computer vision and pattern recognition*. 1780–1789.
- Xiaojie Guo, Yu Li, and Haibin Ling. 2016. LIME: Low-light image enhancement via illumination map estimation. *IEEE Transactions on image processing* 26, 2 (2016), 982–993.
- Jiang Hai, Zhu Xuan, Ren Yang, Yutong Hao, Fengzhu Zou, Fang Lin, and Songchen Han. 2023. R2rnet: Low-light image enhancement via real-low to real-normal network. *Journal of Visual Communication and Image Representation* 90 (2023), 103712.
- Jiang Hai, Ren Yang, Yaqi Yu, and Songchen Han. 2022. Combining Spatial and Frequency Information for Image Deblurring. *IEEE Signal Processing Letters* 29 (2022), 1679–1683.
- Martin Heusel, Hubert Ramsauer, Thomas Unterthiner, Bernhard Nessler, and Sepp Hochreiter. 2017. Gans trained by a two time-scale update rule converge to a local nash equilibrium. *Advances in neural information processing systems* 30 (2017).
- Jonathan Ho, Ajay Jain, and Pieter Abbeel. 2020. Denoising diffusion probabilistic models. *Advances in neural information processing systems* 33 (2020), 6840–6851.
- Hai Jiang, Ao Luo, Haoqiang Fan, Songchen Han, and Shuaicheng Liu. 2023. Low-light image enhancement with wavelet-based diffusion models. *ACM Transactions on Graphics (TOG)* 42, 6 (2023), 1–14.
- Yifan Jiang, Xinyu Gong, Ding Liu, Yu Cheng, Chen Fang, Xiaohui Shen, Jianchao Yang, Pan Zhou, and Zhangyang Wang. 2021. Enlightengan: Deep light enhancement without paired supervision. *IEEE transactions on image processing* 30 (2021), 2340–2349.
- Weicheng Kuo, Yin Cui, Xiuye Gu, AJ Piergiovanni, and Anelia Angelova. 2022. F-vm: Open-vocabulary object detection upon frozen vision and language models. *arXiv preprint arXiv:2209.15639* (2022).

- Chulwoo Lee, Chul Lee, and Chang-Su Kim. 2013. Contrast enhancement based on layered difference representation of 2D histograms. *IEEE transactions on image processing* 22, 12 (2013), 5372–5384.
- Xiaozhou Lei, Zixiang Fei, Wenju Zhou, Huiyu Zhou, and Minrui Fei. 2022. Low-light image enhancement using the cell vibration model. *IEEE Transactions on Multimedia* (2022).
- Chongyi Li, Chunle Guo, and Chen Change Loy. 2021a. Learning to enhance low-light image via zero-reference deep curve estimation. *IEEE Transactions on Pattern Analysis and Machine Intelligence* 44, 8 (2021), 4225–4238.
- Chongyi Li, Chun-Le Guo, Man Zhou, Zhixin Liang, Shangchen Zhou, Ruicheng Feng, and Chen Change Loy. 2023. Embedding fourier for ultra-high-definition low-light image enhancement. *arXiv preprint arXiv:2302.11831* (2023).
- Guofa Li, Yifan Yang, Xingda Qu, Dongpu Cao, and Keqiang Li. 2021b. A deep learning based image enhancement approach for autonomous driving at night. *Knowledge-Based Systems* 213 (2021), 106617.
- Mading Li, Jiaying Liu, Wenhan Yang, Xiaoyan Sun, and Zongming Guo. 2018. Structure-revealing low-light image enhancement via robust retinex model. *IEEE Transactions on Image Processing* 27, 6 (2018), 2828–2841.
- Zhixin Liang, Chongyi Li, Shangchen Zhou, Ruicheng Feng, and Chen Change Loy. 2023. Iterative prompt learning for unsupervised backlit image enhancement. In *Proceedings of the IEEE/CVF International Conference on Computer Vision*. 8094–8103.
- Seokjae Lim and Wonjun Kim. 2020. DSLR: Deep stacked Laplacian restorer for low-light image enhancement. *IEEE Transactions on Multimedia* 23 (2020), 4272–4284.
- Haoning Lin and Zhenwei Shi. 2014. Multi-scale retinex improvement for nighttime image enhancement. *optik* 125, 24 (2014), 7143–7148.
- Risheng Liu, Long Ma, Jiaao Zhang, Xin Fan, and Zhongxuan Luo. 2021. Retinex-inspired unrolling with cooperative prior architecture search for low-light image enhancement. In *Proceedings of the IEEE/CVF Conference on Computer Vision and Pattern Recognition*. 10561–10570.
- Andreas Lugmayr, Martin Danelljan, Andres Romero, Fisher Yu, Radu Timofte, and Luc Van Gool. 2022. Repaint: Inpainting using denoising diffusion probabilistic models. In *Proceedings of the IEEE/CVF Conference on Computer Vision and Pattern Recognition*. 11461–11471.
- Ziwei Luo, Fredrik K Gustafsson, Zheng Zhao, Jens Sjölund, and Thomas B Schön. 2023. Image restoration with mean-reverting stochastic differential equations. *arXiv preprint arXiv:2301.11699* (2023).
- Xiaoqian Lv, Shengping Zhang, Qinglin Liu, Haozhe Xie, Bineng Zhong, and Huiyu Zhou. 2022. BacklitNet: A dataset and network for backlit image enhancement. *Computer Vision and Image Understanding* 218 (2022), 103403.
- Long Ma, Tengyu Ma, Risheng Liu, Xin Fan, and Zhongxuan Luo. 2022. Toward fast, flexible, and robust low-light image enhancement. In *Proceedings of the IEEE/CVF Conference on Computer Vision and Pattern Recognition*. 5637–5646.
- Xiaojiao Mao, Chunhua Shen, and Yu-Bin Yang. 2016. Image restoration using very deep convolutional encoder-decoder networks with symmetric skip connections. *Advances in neural information processing systems* 29 (2016).
- Anish Mittal, Anush Krishna Moorthy, and Alan Conrad Bovik. 2012a. No-reference image quality assessment in the spatial domain. *IEEE Transactions on image processing* 21, 12 (2012), 4695–4708.
- Anish Mittal, Rajiv Soundararajan, and Alan C Bovik. 2012b. Making a “completely blind” image quality analyzer. *IEEE Signal processing letters* 20, 3 (2012), 209–212.
- Ozan Özdenizci and Robert Legenstein. 2023. Restoring vision in adverse weather conditions with patch-based denoising diffusion models. *IEEE Transactions on Pattern Analysis and Machine Intelligence* (2023).
- Jaemin Park, An Gia Vien, Jin-Hwan Kim, and Chul Lee. 2022. Histogram-based transformation function estimation for low-light image enhancement. In *2022 IEEE International Conference on Image Processing (ICIP)*. IEEE, 1–5.
- Mengwei Ren, Mauricio Delbracio, Hossein Talebi, Guido Gerig, and Peyman Milanfar. 2022. Image deblurring with domain generalizable diffusion models. *arXiv preprint arXiv:2212.01789* (2022).
- Chitwan Saharia, William Chan, Huiwen Chang, Chris Lee, Jonathan Ho, Tim Salimans, David Fleet, and Mohammad Norouzi. 2022. Palette: Image-to-image diffusion models. In *ACM SIGGRAPH 2022 Conference Proceedings*. 1–10.
- Jiaming Song, Chenlin Meng, and Stefano Ermon. 2020a. Denoising diffusion implicit models. *arXiv preprint arXiv:2010.02502* (2020).
- Yang Song and Stefano Ermon. 2019. Generative modeling by estimating gradients of the data distribution. *Advances in neural information processing systems* 32 (2019).
- Yang Song, Jascha Sohl-Dickstein, Diederik P Kingma, Abhishek Kumar, Stefano Ermon, and Ben Poole. 2020b. Score-based generative modeling through stochastic differential equations. *arXiv preprint arXiv:2011.13456* (2020).
- Jian Sun, Wenfei Cao, Zongben Xu, and Jean Ponce. 2015. Learning a convolutional neural network for non-uniform motion blur removal. In *Proceedings of the IEEE conference on computer vision and pattern recognition*. 769–777.
- Jianyong Wang, Kelvin CK Chan, and Chen Change Loy. 2023. Exploring clip for assessing the look and feel of images. In *Proceedings of the AAAI Conference on Artificial Intelligence*, Vol. 37. 2555–2563.
- Zhou Wang, Alan C Bovik, Hamid R Sheikh, and Eero P Simoncelli. 2004. Image quality assessment: from error visibility to structural similarity. *IEEE transactions on image processing* 13, 4 (2004), 600–612.
- Zhendong Wang, Xiaodong Cun, Jianmin Bao, Wengang Zhou, Jianzhuang Liu, and Houqiang Li. 2022. Uformer: A general u-shaped transformer for image restoration. In *Proceedings of the IEEE/CVF conference on computer vision and pattern recognition*. 17683–17693.
- Chen Wei, Wenjing Wang, Wenhan Yang, and Jiaying Liu. 2018. Deep retinex decomposition for low-light enhancement. *arXiv preprint arXiv:1808.04560* (2018).
- Wenhui Wu, Jian Weng, Pingping Zhang, Xu Wang, Wenhan Yang, and Jianmin Jiang. 2022. Uretinex-net: Retinex-based deep unfolding network for low-light image enhancement. In *Proceedings of the IEEE/CVF conference on computer vision and pattern recognition*. 5901–5910.
- Xiaogang Xu, Ruixing Wang, Chi-Wing Fu, and Jiaya Jia. 2022. SNR-aware low-light image enhancement. In *Proceedings of the IEEE/CVF conference on computer vision and pattern recognition*. 17714–17724.
- Minglong Xue, Palaiahnakote Shivakumara, Chao Zhang, Yao Xiao, Tong Lu, Umapada Pal, Daniel Lopresti, and Zhibo Yang. 2020. Arbitrarily-oriented text detection in low light natural scene images. *IEEE Transactions on Multimedia* 23 (2020), 2706–2720.
- Wenhan Yang, Shiqi Wang, Yuming Fang, Yue Wang, and Jiaying Liu. 2020. From fidelity to perceptual quality: A semi-supervised approach for low-light image enhancement. In *Proceedings of the IEEE/CVF conference on computer vision and pattern recognition*. 3063–3072.
- Wenhan Yang, Wenjing Wang, Haofeng Huang, Shiqi Wang, and Jiaying Liu. 2021. Sparse gradient regularized deep retinex network for robust low-light image enhancement. *IEEE Transactions on Image Processing* 30 (2021), 2072–2086.
- Syed Waqas Zamir, Aditya Arora, Salman Khan, Munawar Hayat, Fahad Shahbaz Khan, and Ming-Hsuan Yang. 2022. Restormer: Efficient transformer for high-resolution image restoration. In *Proceedings of the IEEE/CVF conference on computer vision and pattern recognition*. 5728–5739.
- Syed Waqas Zamir, Aditya Arora, Salman Khan, Munawar Hayat, Fahad Shahbaz Khan, Ming-Hsuan Yang, and Ling Shao. 2020. Learning

- enriched features for real image restoration and enhancement. In *Computer Vision—ECCV 2020: 16th European Conference, Glasgow, UK, August 23–28, 2020, Proceedings, Part XXV* 16. Springer, 492–511.
- Yuhang Zang, Wei Li, Kaiyang Zhou, Chen Huang, and Chen Change Loy. 2022. Open-vocabulary detr with conditional matching. In *European Conference on Computer Vision*. Springer, 106–122.
- Rongkai Zhang, Lanqing Guo, Siyu Huang, and Bihan Wen. 2021. Relie: Deep reinforcement learning for customized low-light image enhancement. In *Proceedings of the 29th ACM international conference on multimedia*. 2429–2437.
- Richard Zhang, Phillip Isola, Alexei A Efros, Eli Shechtman, and Oliver Wang. 2018. The unreasonable effectiveness of deep features as a perceptual metric. In *Proceedings of the IEEE conference on computer vision and pattern recognition*. 586–595.
- Chong Zhou, Chen Change Loy, and Bo Dai. 2022. Extract free dense labels from clip. In *European Conference on Computer Vision*. Springer, 696–712.